ADVANCED ENGINEERING MATERIALS
www.aem-journal.com

Ag Cluster-Modified $K_{0.5}Na_{0.5}NbO_3$ Piezocatalyst for Enhanced Electrochemical Dinitrogen Reduction Reaction

*Benedict Witulski, Naina Goyal, David Patrun, Fabio Pires, Ziyaad Aytuna, Hamed Alaei, Olav Schiemann, and Sanjay Mathur**

Efforts in finding alternatives to Haber–Bosch process for chemical synthesis of ammonia still struggle with efficient N_2 activation. Piezoelectric materials are promising cocatalysts to enhance the chemical kinetics of dinitrogen (N_2) reduction through, built-in electric fields, upon mechanical activation, which can modulate the surface electrochemical potential. This work reports on the influence of piezoelectric potassium sodium niobate ($K_{0.5}Na_{0.5}NbO_3$, KNN) as a lead-free cocatalyst for the electrochemical nitrogen reduction reaction to ammonia (NH_3) under mild conditions, on a silver (Ag) catalyst. For piezoactivation, modified H-cell is engineered with the working electrode (Ag/KNN), enabling external mechanical actuating during electrochemical process. The results demonstrate that transient dipoles generated on the KNN surface through localized electric field improve threefold NH_3 production (3.6 μg h^{-1} cm^{-2}) and a Faradaic efficiency up to 75%. Piezoinfluence is investigated through actuation-induced, linear sweep voltammetry, electrochemical impedance spectroscopy, chronoamperometry, and open-circuit potential measurements.

1. Introduction

Ammonia (NH_3) is one of the most extensively synthesized chemicals globally, essential for fertilizers, nitrogenous compounds, and dyes.[1–3] It is also a promising hydrogen storage medium due to its high hydrogen content (17.6 wt%) and efficient storage and transport.[4–6] However, cleaving triple bond in a dinitrogen molecule is challenging to its high dissociation energy (940.95 kJ mol^{-1}) and lack of permanent dipole. The industrial Haber–Bosch process transforming N_2 to NH_3 is energy intensive and operates under extreme conditions (10–30 MPa, 400–600 °C) emphasizing the need for alternative routes.[7–9] Electrochemical nitrogen reduction reaction (eNRR) offers a viable alternative for NH_3 synthesis under mild conditions. Noble metals have high yields and high faradaic efficiencies in eNRR, with silver (Ag) emerging as cost-effective candidate,[10] however, Ag-based catalytic systems remain underexplored.[11–16] Recent advances highlight the role of external energy inputs, such as mechanical energy to built-in electric fields via transient surface charges on piezoelectric materials that enhance eNRR kinetics. This phenomenon, fundamental to piezocatalysis, enhances electron transfer process during redox reactions, thereby catalytic efficiency.[17–19] Piezoelectric materials such as $Pb(Zr_xTi_{1-x}O_3)$, $BaTiO_3$, $LiNbO_3$, and $BiFeO_3$ have been utilized in catalytic process like water splitting and organic pollutants degradation, with ultrasonication as the polarization source.[20–28] While nitrogen conversion in piezocatalysis is rarely reported,[29,30] the eNRR has gained significant attention.[31–46]

Herein, we demonstrate the superior efficiency of a piezo-enhanced electrocatalyst in driving the chemical kinetics of eNRR through a piezo-induced built-in electric field.[20–23,25] By coating the electrocatalyst Ag on a lead-free piezoelectric material, potassium sodium niobate ($K_{0.5}Na_{0.5}NbO_3$—KNN) and externally actuating Ag/KNN in a new designed H-cell electrochemical setup, it was possible to significantly improve the eNRR kinetics. The working electrode (Ag/KNN) was actuated at an acoustic vibration of 400 Hz, maximizing the piezoelectric output potential. Comparative study between stationary electrode and actuated electrodes highlights the critical role of piezoelectric activation on modulating catalytic activity. Finally, NH_3 concentration was quantified to assess threefold higher catalytic efficiency of piezo-enhanced reaction,

B. Witulski, N. Goyal, D. Patrun, F. Pires, Z. Aytuna, S. Mathur
Institute of Inorganic and Materials Chemistry
University of Cologne
50939 Cologne, Germany
E-mail: Sanjay.mathur@uni-koeln.de

F. Pires
Brazilian Nanotechnology National Laboratory (LNNano)
Brazilian Center for Research in Energy and Materials (CNPEM) – Campinas
São Paulo 13083-100, Brazil

F. Pires
Institute of Chemistry
State University of Campinas (UNICAMP) – Campinas
São Paulo 13083-100, Brazil

H. Alaei, O. Schiemann
Clausius Institute for Physical and Theoretical Chemistry
University Bonn
53121 Bonn, Germany

The ORCID identification number(s) for the author(s) of this article can be found under https://doi.org/10.1002/adem.202500764.

DOI: 10.1002/adem.202500764

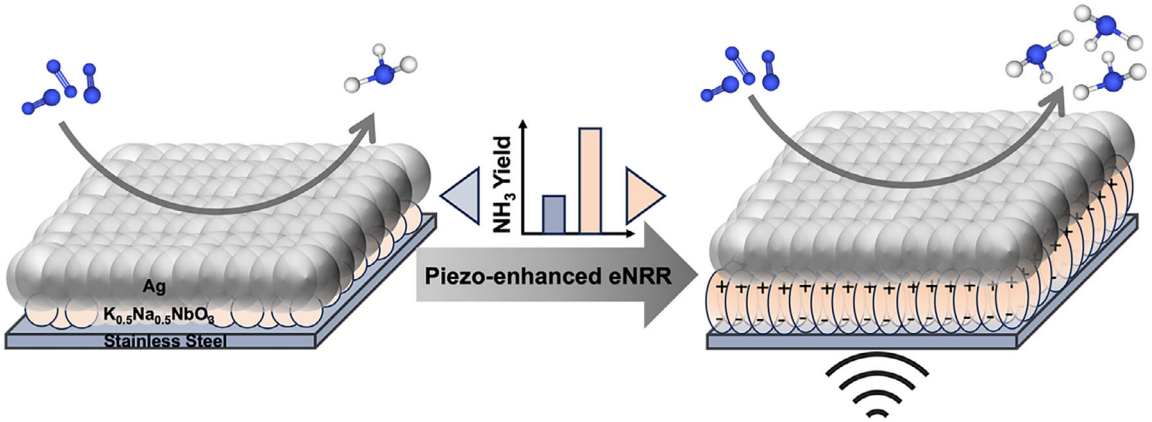

Figure 1. Schematic representation of static and piezoelectrically enhanced electrode yielding more NH_3.

presenting the piezoelectric contributions to eNRR performance (**Figure 1**).

2. Results and Discussion

For the potassium sodium niobate (KNN) synthesis, an equimolar mixture of metal alkoxides was activated by controlled hydrolysis in isopropanol and the resulting sol was concentrated, forming a xerogel. The X-ray diffractogram (XRD) of the as-obtained xerogel shows the amorphous arrangement of the KNN (**Figure 2**a).

Upon calcination at 550 °C for 3 h, the KNN sample demonstrates the formation of a single-phase $K_{0.5}Na_{0.5}NbO_3$ perovskite with orthorhombic phase ($a = 5.65$, b = 3.95 and $c = 5.67$ Å), as confirmed by XRD measurement (Figure 2b). The distinct diffraction profile ($10° < 2\,\theta < 40°$) and the absence of unidentified peaks confirm that no crystalline secondary phase is present.

X-ray photoelectron spectroscopy (XPS) was used to confirm the elemental composition in the KNN samples (**Figure 3**a). The presence of Na, K, and Nb supports the conclusions drawn from XRD and energy-dispersive X-ray spectroscopy (EDX) (Figure S1, Supporting Information). The XPS analysis showed that nitrogen is absent in the as-calcined sample, meaning any ammonia species detected during the catalytic process can be attributed solely to the nitrogen introduced during cell purging. However, a detailed stoichiometry could not be obtained, due to the overlap of the Na 2*s* and Nb 4*s* orbitals observed at 63 and 58 eV, respectively. Since the measuring range is limited to 1000 eV, fitting the Na 1*s* peak at ≈1071 eV was not possible. Carbon (C 1*s*) was also detected, originating from contamination in the machine and signals caused by environmental adsorbates on the sample.[47] Additionally, electron paramagnetic resonance (EPR) spectroscopy measurements were performed to assess the formation of oxygen defects during the KNN synthesis, due to the sublimable nature of alkali metal oxides (Figure 3b).[48] A *g* value of 2.003 confirms the formations of oxygen vacancies during the sol–gel process of KNN, which are crucial in piezocatalysis.[30,49–56]

The morphology of the synthesized KNN was investigated by scanning electron microscopy (SEM), and to achieve a homogeneous coating, a KNN/Nafion solution was prepared using spray coating method onto a stainless-steel substrate (**Figure 4**a). The coating exhibits a macroscopically dense surface morphology constituted by regularly distributed KNN particles with an average layer thickness of 590 nm (Figure 4b and Figure S2, Supporting Information). The resulting piezoelectric film generates a potential of 15 mV, demonstrated by actuation measurements using a custom-made shaker setup with a frequency-controlled surface

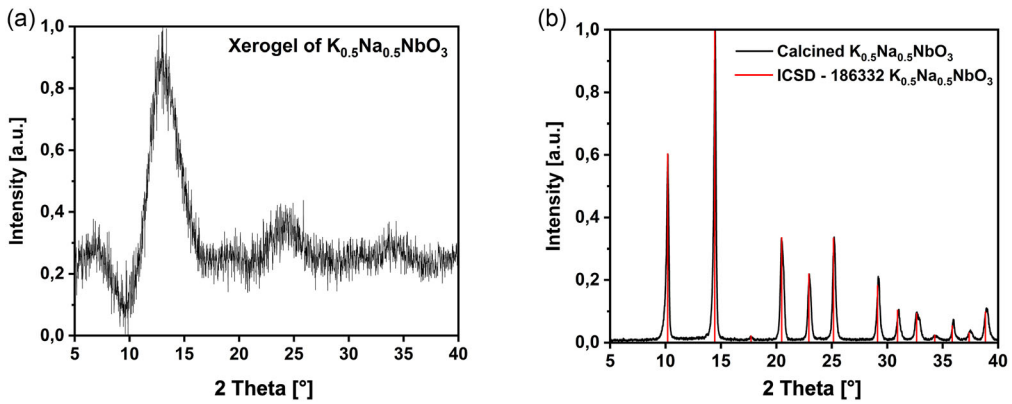

Figure 2. Powder XRD pattern of as-obtained a) amorphous arrangement xerogel of the KNN and b) crystalline KNN after calcination (550 °C).

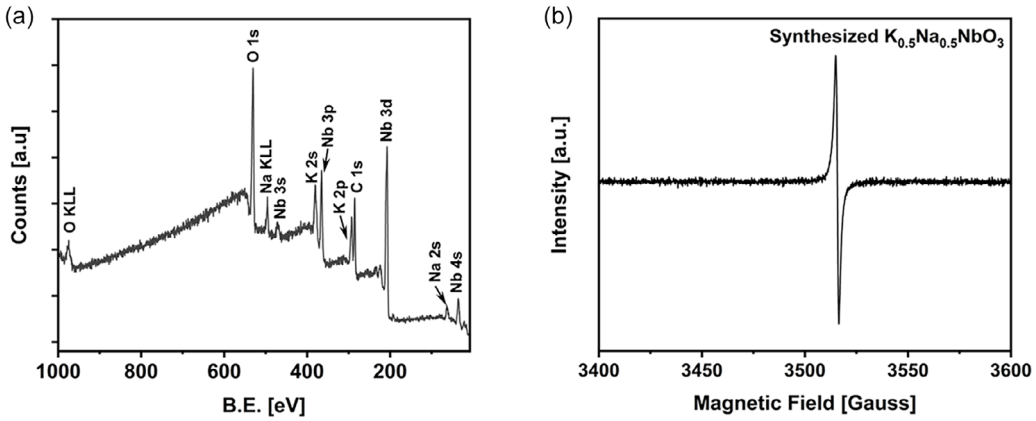

Figure 3. a) XPS survey spectrum of calcined KNN (550 °C). b) Continuous wave X-band electron paramagnetic resonance spectrum of calcined KNN.

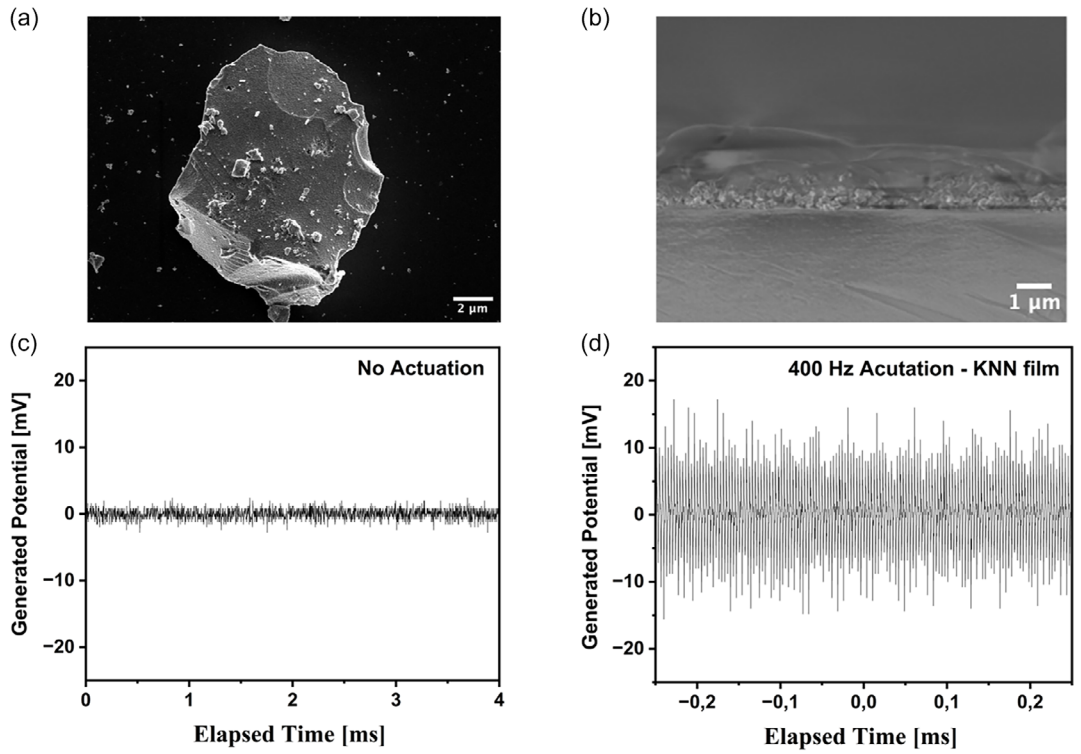

Figure 4. a) SEM micrograph of crystalline KNN particle and b) cross-sectional of the KNN thin film. c) Oscillation measurements without the actuation of KNN film and d) after during actuation at 400 Hz.

speaker of 21.23 cm^2 coupled with a Tektronix TDS 210 two channel digital real-time oscilloscope (Figure 4d). In the absence of actuation, minimal slight noise is observed (Figure 4c). A range of frequencies were examined for optimal piezoactuation, with 400 Hz yielding the highest potential (Figure S3, Supporting Information). The introduction of oxygen vacancies increases the density of free carriers within the material, enhancing the screening effect and hindering polarization.[57] However, actuating measurements reveal a high generated potential in the film, despite the presence of oxygen vacancies, establishing it as a strong candidate for piezoelectrically enhanced electrode.

Due to the poor nitrogen activation from bare KNN (Figure S7, Supporting Information), the piezoelectric layer functions as a cocatalyst for the sputtered Ag thin film (20 nm). To determine the optimal ratio of Ag to the KNN cocatalyst, the Ag nanolayer thickness was optimized using different thicknesses achieved by adjusting the sputtering durations (Figure S4, Supporting Information). The 20 nm thick layer of Ag delivered the best catalytic performance. For integration into an H-cell electrochemical setup, the piezoelectric working electrode was positioned on the side of the cell, enabling external actuation at the corresponding frequency and promoting the interaction between the

reactant and the catalyst on highly actuated catalytic surfaces (**Figure 5**a). The electric polarization in response to mechanical stress creates charges on the surface of the material. This continuous stress-induced polarization induced by mechanical stress creates transient dipoles and a piezopotential in the material, creating a built-in electric field. This effect can improve catalytic reactions and enhance efficiency.[52–54,58,59]

An electrochemical comparison of chronoamperometry, impedance, and open-circuit potential (OCP) was conducted in 0.1 M Na_2SO_4 between the bare Ag electrocatalyst, the piezoelectric Ag/KNN electrode, and the perovskite-based nonpiezoelectric reference Ag/$SrTiO_3$ (Figure 5). Although $SrTiO_3$ can exhibit piezoelectric properties under specific conditions, synthesis routes, or structural modifications, the $SrTiO_3$ in this study is a commercially available material exhibiting a cubic phase with space group *Pm-3m*. This centrosymmetric structure lacks of any piezoelectric properties at room temperature (Figure S8, Supporting Information).[60–63] The electrochemical comparison highlights the influence of the built-in electric field on the piezoelectrically enhanced electrode. Figure 5 illustrates the electrochemical change of potential when actuation is applied to the piezo-enhanced Ag/KNN electrode. Chronoamperometry analysis (Figure 5d) showed an increase in current of about 40 µA when the piezoelectrically enhanced electrode was continually actuated. In comparison, Ag/$SrTiO_3$ and Ag electrocatalysts show no effect on the measured current. Electrochemical impedance spectroscopy (EIS) measurements were performed to estimate the charge transfer of composite electrodes with and without actuation. The Nyquist plots were fitted using a Voigt-like circuit (Figure 5c). Composed of R_0 for the stainless-steel substrate resistance, CPE//R_1 for the impedance at the Ag/KNN interface, and CPE//R_2 as the impedance between the catalyst surface and the electrolyte. Upon mechanical actuation, R_0 remained constant at ≈25 Ω, while the resistance at the electrode/electrolyte interface is reduced from 173 to 132 Ω. The results from chronoamperometry and EIS confirm an increase in charge transfer. Transient OCP measurements exhibit negligible voltage variation for Ag and Ag/$SrTiO_3$ with or without actuation, while Ag/KNN exhibits a piezovoltage of 33 mV (Figure 5b). These results further corroborate the creation of a built-in electric field during actuation attributed to a surface polarization of KNN rather than creation of additional charge carriers.[64]

Linear sweep voltammetry (LSV) was measured using Ar and N_2 as feeding gas for 30 min each. The N_2-saturated solution exhibits higher negative current indicating electrocatalytic activity toward eNRR. As expected, the higher current upon actuating the piezoelectric electrode suggests increased electron migration

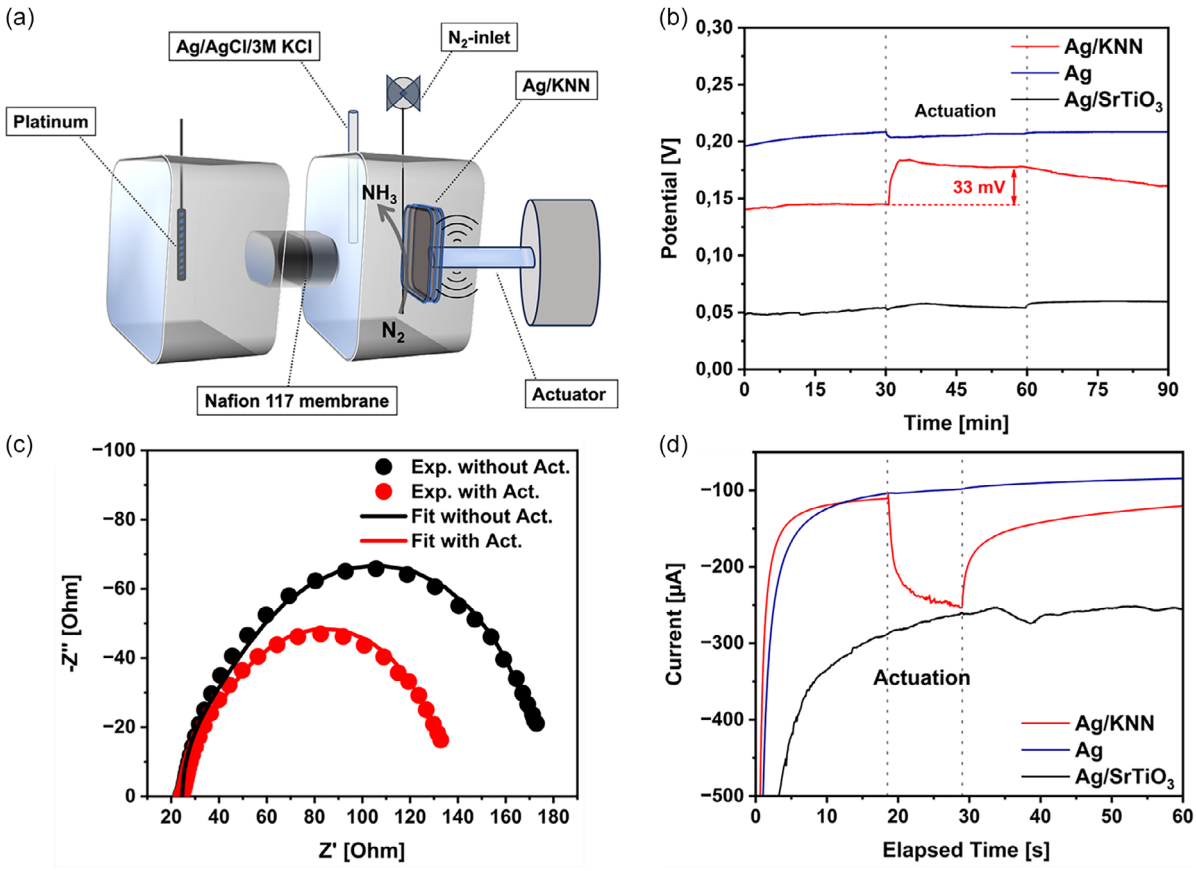

Figure 5. a) Schematic representation of developed H-cell electrochemical setup. b) Differentiation of Ag/KNN, Ag, and Ag/$SrTiO_3$ in measured OCP, c) Nyquist plots EIS measurements of the piezoelectric working electrode without/with actuation, and d) chronoamperometry of Ag/KNN, Ag, and Ag/$SrTiO_3$ without/with actuation.

to the electrode surface, thereby enhancing participation in the eNRR (**Figure 6**a). The performance of bare KNN does not qualify it as an efficient catalyst for nitrogen reduction, as shown in the LSV (Supporting Information, Figure S7). Chronoamperometry measurements at −0.2 V versus RHE were conducted for 2 h, comparing static and actuated Ag/KNN electrode states (Figure 6b). Notably, the current density remained stable under both conditions throughout catalysis. The amount of in situ generated NH_3 was quantified using the indophenol method and to the NH_4^+ calibration curve (Figure S5, Supporting Information), while formation of potential N_2H_4 by-products was determined using the Watt-and-Crisp method (Figure S6, Supporting Information).[65] Figure 6c illustrates the indophenol method enhancement in NH_3 quantification through piezo-assisted nitrogen activation, showing a threefold increase in the absorbed peak when a highly actuated piezoelectric electrode is used.

The static piezoelectric electrode quantifies 1.21 μg h^{-1} cm^{-2} produced NH_3, whereas the piezoelectrically enhanced electrode achieves an impressive 3.6 μg h^{-1} cm^{-2} NH_3 yield, representing a remarkable threefold improvement in piezo-assisted eNRR and marking the highest NH_3 yield attained in comparison with static and actuated bare KNN, Ag, Ag/$SrTiO_3$, and Ag/KNN electrodes. Additionally, the Faradaic efficiency (FE) experiences also a remarkable increase, from 18% with a static electrode to 75% achieved by using piezoelectrically enhanced electrode.

The bare Ag electrode demonstrates an NH_3 yield of 1.94 μg h^{-1} cm^{-2}, however, the introduction of an actuated electrode results in a reduction in performance of 1.13 μg h^{-1} cm^{-2}. Not only the NH_3 yield of the Ag electrode declined due to actuation, but the FE also decreased with the actuated Ag electrode. The nonpiezoelectric electrode using Ag/$SrTiO_3$ as a perovskite layer shows an NH_3 yield of 1.75 μg h^{-1} cm^{-2}, with no difference observed between actuated and static conditions.

The catalyst was also structurally and morphologically characterized after catalysis. Morphological evaluation via SEM imaging, before and after catalysis, reveals a consistently rough surface composed of KNN particles varying sizes. Although the surface roughness of the particles changes slightly, overall morphology of the film and crystallinity of KNN remains intact (**Figure 7**a,b). The XRD analysis demonstrates that the piezoelectric material KNN retains its crystalline structure after catalysis, as all diffraction peaks remain unchanged (Figure 7c). This corroborates a stability which is further supported by long-term chronoamperometry measurements conducted over 24 h period, during which the current density remained consistently stable (Figure 7d).

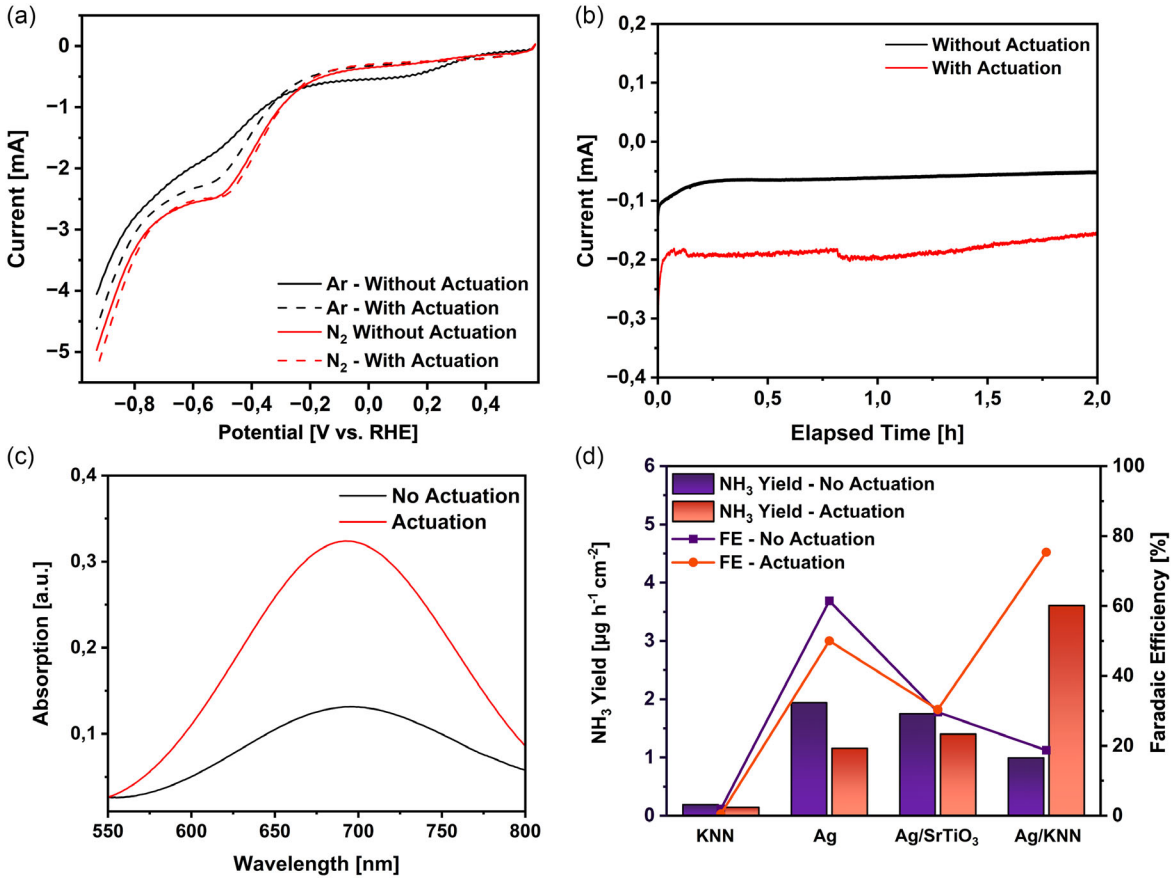

Figure 6. a) LSV curves of the piezoelectric working electrode Ar-, N_2-saturated solution with and without actuation. b) Chronoamperometry of the 2 h reaction period with and without actuation. c) Comparison of the UV–vis absorption spectra of the indophenol indicator for static and actuated electrode. d) NH_3 yield rates and FE comparing KNN, Ag, Ag/$SrTiO_3$, Ag/KNN as static electrode as well as actuated electrode.

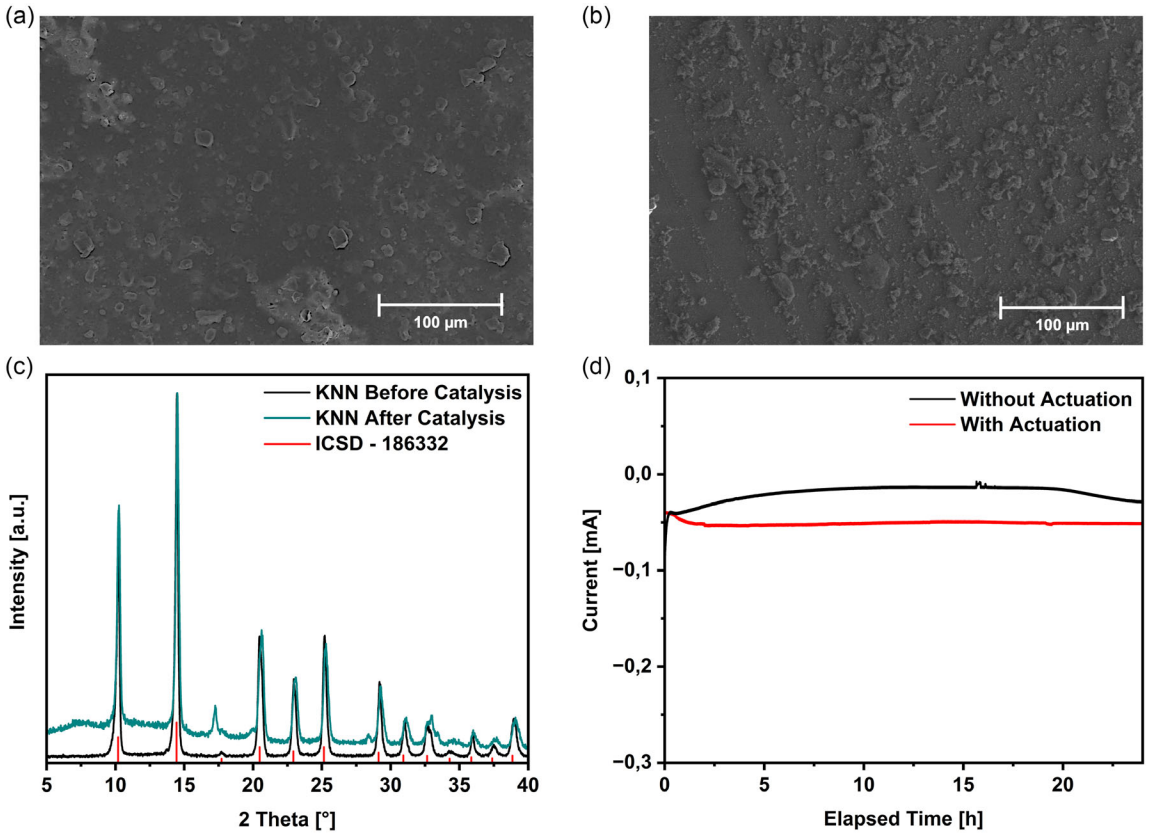

Figure 7. SEM micrographs of the catalyst film a) before catalysis and b) after catalysis. c)XRD pattern of KNN film before and after catalysis. d) Long-term chronoamperometry of the 24 h reaction period with and without actuation.

3. Conclusion

In summary, the piezoelectric material potassium sodium niobate ($K_{0.5}Na_{0.5}NbO_3$, KNN) was successfully synthesized via the sol–gel method using potassium *tert*-butoxide, sodium *tert*-butoxide, and niobium *iso*-propoxide as alkoxide precursors. The synthesized KNN, containing oxygen vacancies, was utilized as an active material and cocatalyst, integrated within a Nafion dispersion and deposited onto stainless-steel substrate via spray coating. Although oxygen vacancies increases the density of free carriers within the material, enhancing the screening effect and hindering polarization, actuation measurements show uniform potential generation of 10−15 mV at a frequency of 400 Hz, confirming the piezoelectric functionality. Furthermore, Ag was deposited onto the electrode to facilitate the eNRR. The piezoelectric working electrode was positioned on the side of an engineered electrochemical cell enabling external actuation and the role of the piezoelectric Ag/KNN in the electrochemical system was systematically evaluated using chronoamperometry, impedance spectroscopy and OCP, compared to bare Ag electrocatalyst and nonpiezoelectric perovskite $Ag/SrTiO_3$. The piezo-assisted electrocatalytic system demonstrated a significant enhancement in the conversion of N_2 to NH_3 under neutral conditions (0.1 M Na_2SO_4), achieving an ammonia yield three times higher than that of the reference systems and a FE of 75% at mild applied potential of −0.2 V versus RHE over a 2 h reaction period. These finding highlight the synergistic effect of piezoelectric KNN in driving electrochemical nitrogen activation and underscore its potential as a promising multifunctional material for sustainable and efficient ammonia synthesis under mild conditions. Furthermore, structural and morphological analysis after catalysis were done, showing high stability in crystallinity and morphology. This stability was further confirmed by 24 h long-term chronoamperometry using both actuated and nonactuated electrode, exhibiting consistent performance throughout the measurement period.

4. Experimental Section

The synthesis of metal alkoxide precursor was conducted under an inert nitrogen atmosphere using a Stock vacuum line equipped with quick-fit glass joints. All alkoxides were purified by sublimation, and solvents were freshly distilled over freshly cut sodium. Stainless-steel sheets with a thickness of 0.15 mm (Good Fellow, Fe/Cr18/Ni10)) were used as substrates. The XRD experiments were performed using the following diffractometer: capillary measurement in Debye–Scherrer geometry on a STOE STADI P diffractometer, equipped with a Dectris Mythen 1 detector using λ_{Mo} $K_\alpha = 0.70930$ Å radiation. The surface composition was analyzed by using XPS with an ESCA M-Probe (Surface Science Instruments) equipped with an Al Kα source. Data processing was performed using CasaXPS software (Casa Software Ltd.), calibrated to the adventitious carbon signal at 248.8 eV. EPR measurements were performed using a continuous wave X-band EPR spectrometer EMXmicro from Bruker in combination with a SHQ resonator also from Bruker. The morphology and bulk elemental distribution were analyzed by using a Zeiss Sigma 300 VP Rise field

emission SEM with integrated EDX (Oxford Instruments Xplore 30). Electrochemical measurements, including EIS, chronoamperometry, linear sweep voltammetry, and OCP were conducted by using the potentiostat PalmSens4 from PalmSens.

Materials Synthesis: The Supporting Information is referenced to provide further details of the synthesis of $[Nb(O^iPr)_5]_2$. The piezoelectric, $K_{0.5}Na_{0.5}NbO_3$ (KNN), was synthesized via a sol–gel method using potassium *tert*-butoxide (KO^tBu, Sigma–Aldrich, 97%), sodium *tert*-butoxide (NaO^tBu, Sigma–Aldrich, 98%), and niobium iso-propoxide $[Nb(O^iPr)_5]_2$ as alkoxide precursors. Although the targeted stoichiometry corresponds to a 1:1:1 molar ratio of K:Na:Nb, a 1:1:2 ratio was employed to account for the dimeric nature of niobium iso-propoxide $[Nb(O^iPr)_5]_2$, which contains two Nb centers per molecule.[66–69] In a typical synthesis, KO^tBu (160 mg, 1.43 mmol), NaOtBu (137 mg, 1.43 mmol), and $[Nb(O^iPr)_5]_2$ (1.11 g, 1.43 mmol) were dissolved in 10 mL HO^iPr (anhydrous 99.8%). The solution was stirred for 2 h at room temperature followed by the addition of 10 mL acetic acid (Analytical reagent grade, Fisher Chemicals). The solution was stirred for additional 12 h, before drying at 140 °C. The resulting xerogel was then calcined at 550 °C for 3 h.

Piezoelectric Working Electrode Preparation: Samples for electrochemical studies were prepared by spray-coating a KNN, iso-propylalcohol, 1% V/V Nafion solution onto a stainless-steel substrate. The solution containing the piezoelectric working electrode was prepared as follows: 60 mg of the calcined KNN powder was dispersed in 20 mL iso-propylalcohol and 1% V/V Nafion D-521 Dispersion (5% w/w in H_2O and iso-propyalcohol, Alfa Aesar) solution was added. After homogenous dispersion in an ultrasonic bath, the active material was loaded onto a 4.9 $cm^2 \times 0.15$ mm stainless-steel (Fe/Cr18/Ni10) substrate via spray coating. Finally, a 20 nm silver layer was deposited onto the piezoelectric working electrode by magnetron sputtering under Ar (99.99%) atmosphere (14 s, 120 mA, 20 nm). The $SrTiO_3$ used as reference material, structurally a perovskite, but non-piezoelectric was purchased from the company Chempur. The catalyst fabrication followed the same procedure as used for the KNN-based system.

Electrochemical Measurements: Electrochemical investigation including eNRR was performed in a three-electrode system (H-type two-chamber cell), with platinum serving as the counter electrode, Ag/AgCl (3 M KCl) as the reference electrode, and the fabricated working electrode positioned adjacent to the side of the electrochemical cell. According to the Nernst equation:[37]

$$E_{RHE} = E_{Ag/AgCl} + 0.197 + 0.059\,pH \quad (1)$$

The system was purged with argon (Ar) gas for 30 min, followed by additional 30 min of nitrogen (N_2) flushing with the quantitative assessment through chronoamperometry at constant potential of −0.2 V versus RHE in 0.1 M Na_2SO_4 solution. Pure N_2 was consistently introduced into the cathode chamber during catalysis. Equation (2) was utilized for calculation of the produced NH_3 amount in 40 mL cathode electrolyte, where R_{NH3} ($\mu g\,h^{-1}\,cm^{-2}$) represents the NH_3 production rate, C_{NH3} is the NH_3 concentration in the detection solution in ppm (μg/mL), V (mL) denotes the volume of the cathode electrolyte, t (h) is the catalysis time, and A (cm^2) describes the area of the electrode.

$$R_{NH_3}[\mu g\,h^{-1}cm^{-2}] = \frac{C_{NH_3} \cdot V}{t \cdot A} \quad (2)$$

The FE was calculated as follows:

$$FE = \frac{n\,NH_3 \cdot 3F}{Q} \quad (3)$$

n NH_3 (mol) is the number of moles that where produced, where F(96 485 $C\,mol^{-1}$) describes the Faraday constant and Q(C) is the total electrical charge during the eNRR process.

NH_3 Determination: The concentration of generated NH_3 was analyzed by using the indophenol spectrophotometry method.[36] For the analysis, 2.5 mL of the electrolyte extracted from the cathode chamber postcatalysis was subjected to coloration using the indophenol method. After homogenization, the solution was set to rest for 10 min. The UV–vis absorption of the NH_3-containing electrolyte was measured at 692 nm. Figure S5, Supporting Information, depicts the concentration/absorbance relationship of a linear standard curve ($R = 0.99704$) utilizing varying concentrations of standard ammonium chloride solution.

Supporting Information

Supporting Information is available from the Wiley Online Library or from the author.

Acknowledgements

The authors gratefully acknowledge the financial and infrastructural support provided by the University of Cologne and the German Science Foundation (DFG). Dr. Touraj Karimpour is thankfully acknowledged for contributing with scientific discussions to the final version of this work. F.A.P. also acknowledges the São Paulo Research Foundation (FAPESP grant no. 2024/05567-3).

Open Access funding enabled and organized by Projekt DEAL.

Conflict of Interest

The authors declare no conflict of interest.

Author Contributions

Benedict Witulski: conceptualization (equal); data curation (equal); formal analysis (equal); investigation (lead); methodology (lead); validation (lead); visualization (lead); writing—original draft (lead). **Naina Goyal**: conceptualization (supporting); data curation (supporting); formal analysis (supporting); methodology (supporting); writing—review and editing (supporting). **David Patrun**: data curation (supporting); formal analysis (supporting); investigation (supporting); software (supporting); validation (supporting). **Fabio Pires**: data curation (supporting); formal analysis (supporting); investigation (supporting); methodology (supporting); validation (supporting); visualization (supporting); writing—review and editing (supporting). **Ziyaad Aytuna**: data curation (supporting); formal analysis (supporting); investigation (supporting); validation (supporting). **Hamed Alaei**: formal analysis (supporting); methodology (supporting); validation (supporting). **Olav Schiemann:** formal analysis (supporting); investigation (supporting); methodology (supporting). **Sanjay Mathur:** conceptualization (lead); funding acquisition (lead); methodology (equal); project administration (lead); resources (lead); supervision (lead); validation (equal); writing—review and editing (lead).

Data Availability Statement

The data that support the findings of this study are available from the corresponding author upon reasonable request.

Keywords

piezocatalysis, piezo assisted electrochemical nitrogen reduction reaction, piezo enhanced ammonia synthesis, sol-gel, metal alkoxide

Received: March 18, 2025
Revised: June 5, 2025
Published online: July 4, 2025

[1] T. M. Edwards, H. J. Puglis, D. B. Kent, J. L. Durán, L. M. Bradshaw, A. M. Farag, *Sci. Total Environ.* **2024**, *907*, 167911.
[2] H. Ishaq, C. Crawford, *Energy Convers. Manag.* **2024**, *300*, 117869.
[3] Z. Huang, M. Rafiq, A. R. Woldu, Q. X. Tong, D. Astruc, L. Hu, *Coord. Chem. Rev.* **2023**, *478*, 214981.
[4] R. Lan, J. T. S. Irvine, S. Tao, *Int. J. Hydrogen Energy* **2011**, *37*, 1482.
[5] N. Ma, W. Zhao, W. Wang, X. Li, H. Zhou, *Int. J. Hydrogen Energy* **2024**, *50*, 379.
[6] V. Negro, M. Noussan, D. Chiaramonti, *Energies* **2023**, *16*, 16176192.
[7] M. Aziz, A. TriWijayanta, A. B. D. Nandiyanto, *Energies* **2020**, *13*, 3062.
[8] N. Erfani, L. Baharudin, M. Watson, *Chem. Eng. Process. - Process Intensif.* **2024**, *204*, 109962.
[9] E. Castillejos, E. García-Bordejé, *ChemCatChem* **2024**, *16*, 202301603.
[10] X. Long, F. Huang, Z. Yao, P. Li, T. Zhong, H. Zhao, S. Tian, D. Shu, C. He, *Small* **2024**, *20*, 00551.
[11] W. Li, K. Li, Y. Ye, S. Zhang, Y. Liu, G. Wang, C. Liang, H. Zhang, H. Zhao, *Commun. Chem.* **2021**, *4*, 1.
[12] L. Ji, X. Shi, A. M. Asiri, B. Zheng, X. Sun, *Inorg. Chem.* **2018**, *57*, 14692.
[13] W. Y. Gao, Y. C. Hao, X. Su, L. W. Chen, T. A. Bu, N. Zhang, Z. L. Yu, Z. Zhu, A. X. Yin, *Chem. Commun.* **2019**, *55*, 10705.
[14] Y. Chen, R. Guo, X. Peng, X. Wang, X. Liu, J. Ren, J. He, L. Zhuo, J. Sun, Y. Liu, Y. Wu, J. Luo, *ACS Nano* **2020**, *14*, 6938.
[15] H. Yu, Z. Wang, D. Yang, X. Qian, Y. Xu, X. Li, H. Wang, L. Wang, *J. Mater. Chem. A* **2019**, *7*, 12526.
[16] H. Huang, L. Xia, X. Shi, A. M. Asiri, X. Sun, R. Li, *Chem. Commun.* **2018**, *54*, 11427.
[17] S. Tu, Y. Guo, Y. Zhang, C. Hu, T. Zhang, T. Ma, H. Huang, *Adv. Funct. Mater.* **2020**, *30*, 1.
[18] W. Wu, S. Liang, Y. Chen, L. Shen, R. Yuan, L. Wu, *Mater. Res. Bull.* **2013**, *48*, 1618.
[19] M. Du, W. Liu, N. Liu, Y. Ling, S. Kang, *Nano Energy* **2024**, *124*, 109495.
[20] Y. Ehrnst, P. C. Sherrell, A. R. Rezk, L. Y. Yeo, *Adv. Energy Mater.* **2023**, *13*, 2203164.
[21] Y. Feng, L. Ling, Y. Wang, Z. Xu, F. Cao, H. Li, Z. Bian, *Nano Energy* **2017**, *40*, 481.
[22] L. Qifeng, M. Jingjun, M. Sharma, R. Vaish, *J. Am. Ceram. Soc.* **2019**, *102*, 5807.
[23] S. Lan, J. Feng, Y. Xiong, S. Tian, S. Liu, L. Kong, *Environ. Sci. Technol.* **2017**, *51*, 6560.
[24] D. Shao, L. Zhang, S. Sun, W. Wang, *ChemSusChem* **2018**, *11*, 527.
[25] H. You, Y. Jia, Z. Wu, X. Xu, W. Qian, Y. Xia, M. Ismail, *Electrochem. Commun.* **2017**, *79*, 55.
[26] L. Hao, H. Huang, Y. Guo, Y. Zhang, *ACS Sustainable Chem. Eng.* **2018**, *6*, 1848.
[27] S. Tu, H. Huang, T. Zhang, Y. Zhang, *Appl. Catal., B* **2017**, *219*, 550.
[28] H. Huang, S. Tu, C. Zeng, T. Zhang, A. H. Reshak, Y. Zhang, *Angew. Chem., Int. Ed.* **2017**, *56*, 11860.
[29] M. Frank, Y. Bulut, L. Czympiel, R. Weißing, V. Nahrstedt, M. Wilhelm, M. Grosch, A. Raauf, A. Verma, T. Fischer, S. Mathur, *Nanotechnology* **2021**, *32*, 465601.
[30] J. Yuan, W. Feng, Y. Zhang, J. Xiao, X. Zhang, Y. Wu, W. Ni, H. Huang, W. Dai, J. Yuan, J. Xiao, X. Zhang, Y. Wu, W. Ni, W. Dai, W. Feng, Y. Zhang, H. Huang, *Adv. Mater.* **2024**, *36*, 2303845.
[31] Y. Shiraishi, M. Hashimoto, K. Chishiro, K. Moriyama, S. Tanaka, T. Hirai, *J. Am. Chem. Soc.* **2020**, *142*, 7574.
[32] Z. Zhao, C. Choi, S. Hong, H. Shen, C. Yan, J. Masa, Y. Jung, J. Qiu, Z. Sun, *Nano Energy* **2020**, *78*, 105368.
[33] X. Ren, M. Xia, B. Chong, X. Yan, N. Wells, G. Yang, *Appl. Catal., B* **2021**, *297*, 120468.
[34] J. Li, D. Wang, R. Guan, Y. Zhang, Z. Zhao, H. Zhai, Z. Sun, *ACS Sustainable Chem. Eng.* **2020**, *8*, 18258.
[35] H. K. Lee, C. S. L. Koh, Y. H. Lee, C. Liu, I. Y. Phang, X. Han, C. K. Tsung, X. Y. Ling, *Sci. Adv.* **2018**, *4*.
[36] Y. Zhao, F. Wu, Y. Miao, C. Zhou, N. Xu, R. Shi, L. Z. Wu, J. Tang, T. Zhang, *Angew. Chem.,- Int. Ed.* **2021**, *60*, 21728.
[37] R. Tang, S. Zhou, L. Zhang, L. Yin, *Adv. Funct. Mater.* **2018**, *28*, 1706154.
[38] X. Guo, H. Du, F. Qu, J. Li, *J. Mater. Chem. A* **2019**, *7*, 3531.
[39] X. Zhao, G. Hu, G. F. Chen, H. Zhang, S. Zhang, H. Wang, *Adv. Mater.* **2021**, *33*, 202007650.
[40] M. S. Yu, S. C. Jesudass, S. Surendran, J. Y. Kim, U. Sim, M. K. Han, *ACS Appl. Mater. Interfaces* **2022**, *14*, 31889.
[41] K. Ithisuphalap, H. Zhang, L. Guo, Q. Yang, H. Yang, G. Wu, *Small Methods* **2019**, *3*.
[42] M. H. Vu, C. C. Nguyen, T. O. Do, *ACS Sustainable Chem. Eng.* **2020**, *8*, 12321.
[43] D. Sun, H. Bai, Y. Zhao, Q. Zhang, Y. Bai, Y. Liu, X. Pang, F. Wang, J. Ding, D. Xu, W. Fan, W. Shi, *ACS Appl. Mater. Interfaces* **2020**, *12*, 52763.
[44] M. Li, Q. Lu, M. Liu, P. Yin, C. Wu, H. Li, Y. Zhang, S. Yao, *ACS Appl. Mater. Interfaces* **2020**, *12*, 38266.
[45] R. Karimi, F. Yousefi, M. Ghaedi, K. Dashtian, G. Yasin, *J. Environ. Chem. Eng.* **2022**, *10*, 108549.
[46] J. Zheng, Y. Lyu, J. P. Veder, B. Johannessen, R. Wang, R. De Marco, A. Huang, S. P. Jiang, S. Wang, *J. Phys. Chem. C* **2021**, *125*, 23041.
[47] T. L. Barr, S. Seal, *J. Vac. Sci. Technol. A* **1995**, *13*, 1239.
[48] M. F. Butman, A. A. Smirnov, L. S. Kudin, Z. A. Munir, *Philos. Mag. B* **2000**, *80*, 1653.
[49] Y. Xu, H. Y. Xu, L. W. Shan, Y. Liu, M. C. Cao, L. G. Jin, L. M. Dong, *Inorg. Chem.* **2024**, *63*, 6500.
[50] X. Shi, L. Li, Q. Zhu, C. Chen, C. Wang, *J. Alloys Compd.* **2024**, *987*, 174218.
[51] T. Yang, J. Wei, Z. Sun, Y. Li, Z. Liu, Y. Xu, G. Chen, T. Wang, H. Sun, Z. Cheng, *Appl. Surf. Sci.* **2022**, *575*, 151713.
[52] D. Gao, Z. Dong, W. Feng, Z. Li, H. Wu, Y. Wu, Q. Wei, C. Meng, Y. Wu, Y. Wang, L. Xu, X. Cao, Z. Zhang, Y. Liu, *Inorg. Chem.* **2024**, *63*, 5931.
[53] Z. Wei, T. Ji, X. Zhou, J. Guo, X. Yu, H. Liu, J. Wang, *Small* **2023**, *19*, 2304202.
[54] Y. Xiang, C. Zhao, J. Zhang, K. Jia, Y. Yin, N. Wen, J. Liu, Z. Li, G. Wang, *Appl. Catal., A* **2024**, *688*, 119978.
[55] K. Chu, W. Zong, G. Xue, H. Guo, J. Qin, H. Zhu, N. Zhang, Z. Tian, H. Dong, Y.-E. Miao, M. B. J. Roeffaers, J. Hofkens, F. Lai, T. Liu, *Cite This: J. Am. Chem. Soc.* **2023**, *145*, 21387.
[56] J. Nan, Y. Fang, K. Rong, Y. Liu, S. Dong, *Appl. Catal., B* **2024**, *357*, 124328.
[57] H. Dong, Y. Zhou, L. Wang, L. Chen, M. Zhu, *Chem. Eng. J.* **2024**, *487*, 150480.
[58] J. He, C. Dong, X. Chen, H. Cai, X. Chen, X. Jiang, Y. Zhang, A. Peng, M. A. H. Badsha, *Crystals* **2023**, *13*, 1382.
[59] Y. Wu, H. Shangs, X. Pan, G. Zhou, *Mol. Catal.* **2024**, *556*, 113820.
[60] J. Ling, K. Wang, Z. Wang, H. Huang, G. Zhang, *Ultrason. Sonochem.* **2020**, *61*, 104819.
[61] Y. Jiang, M. Li, Y. Mi, L. Guo, W. Fang, X. Zeng, T. Zhou, Y. Liu, *Nano Energy* **2021**, *85*, 105949.
[62] N. F. Muhamad, R. A. Maulat Osman, M. S. Idris, M. N. Mohd Yasin, in *EPJ Web Conf.*, EDP Sciences, Les Ulis, France **2017**.
[63] A. Erba, K. E. El-Kelany, M. Ferrero, I. Baraille, M. Rérat, *Phys. Rev. B: Condens. Matter Mater. Phys.* **2013**, *88*, 035102.
[64] L. Chen, J.-T. Ren, Z.-Y. Yuan, L. Chen, J.-T. Ren, Z.-Y. Yuan, *Adv. Energy Mater.* **2023**, *13*, 2203720.

[65] J. Chi, L. Guo, J. Mao, T. Cui, J. Zhu, Y. Xia, J. Lai, L. Wang, *Adv. Funct. Mater.* **2023**, *33*, 2300625.
[66] N. Y. Turova, E. P. Turevskaya, V. G. Kessler, M. I. Yanovskaya, *The Chemistry of Metal Alkoxides*, Springer Science & Business Media, Berlin **2007**.
[67] B. D. C. Bradley, B. N. Chakravarti, W. Wardlaw, *J. Chem. Soc.* **1956**, *1956*, 2381.
[68] W. J. Evans, M. S. Sollberger, J. W. Ziller, *J. Am. Chem. Soc* **1993**, *115*, 4120.
[69] D. E. Pearsont, C. A. Buehler, *Chem. Rev.* **1974**, *74*, 45.